Appendix A

Propane Dehydrogenation on $V_4O_{10}^+$

A.1 Introduction

The chemical reactivity of gas phase size-selected vanadium oxide cluster ions with hydrocarbons in a collision cell was systematically investigated by Schwarz et al. [184, 288–290] and by Castleman et al. [99, 106, 114, 291]. They demonstrated that the reaction channels and reaction speeds strongly depend on the cluster size and charge state as well as on the oxygen content. Upon reaction of vanadium oxide cluster ions with alkanes and alkenes several reaction pathways have been observed such as (i) molecular association, (ii) electron transfer, (iii) hydride transfer, (iv) oxygen loss reactions, (v) C$-$C bond cleavage followed by the elimination of ethane, and (vi) oxidative dehydrogenation.

The lack of experimentally determined structures together with the lack of thermochemical data, however, has hindered the identification of structure-reactivity relationships. The size and composition of the reactants and products can be characterized using mass spectrometry. Their geometric structures can, in principle, be predicted by quantum chemical approaches. In practice, the reliable structure prediction is complicated by the lack of an algorithm for finding the absolute energy minimum on a complex potential energy surface.

The reactivity of $V_4O_{10}^+$ is of particular interest. A notable result is the ability of $V_4O_{10}^+$ to thermally activate methane, resulting in the abstraction of one hydrogen atom and a barrier-less production of the hydroxide cluster cation $V_4O_9(OH)^+$ concomitant with a neutral methyl radical [184]. $V_4O_{10}^+$ also oxidizes ethylene to produce acetaldehyde [99, 114, 291] and oxidatively dehydrogenates small alkanes resulting in the formal $V_4O_{10}H_2^+$ concomitant with the elimination of the respective alkenes [288]. The structure of $V_4O_{10}^+$ is a tetrahedral cage with bridging oxygen

atoms on the edges, vanadyl groups, V=O, at three corners, and an oxygen centered radical, resulting in one long terminal V−O bond of 1.75 Å, versus terminal vanadyl V=O bonds of 1.56 Å (see Figure A.1). The spin density has the shape of a p orbital and is mainly localized at the radical oxygen site, which determines the high reactivity of $V_4O_{10}^+$ [114, 184]. The complexity and size specificity of these reactions causes interest in the underlying reaction mechanisms as well as in the structures of the vanadium oxide cluster–molecule complexes. Vibrational spectroscopy in combination with density functional calculations has assigned the structures of small cationic and anionic vanadium oxide clusters [54, 104, 113, 292]. However, with the exception of $V_2O_5(C_2H_4)^+$ and $V_2O_6(C_2H_4)^+$ [293], no direct experimental characterization of the structure of metal oxide cluster–hydrocarbon complexes has been reported. Most existing structural information is indirect and mainly based on chemical reactivity measurements in combination with computational approaches. Here, the reaction of $V_4O_{10}^+$ with propane is studied by IR-PD spectroscopy. Mass selected $V_4O_{10}^+$ clusters react with propane in the ion trap and IR-PD spectra are measured for reaction intermediates and products.
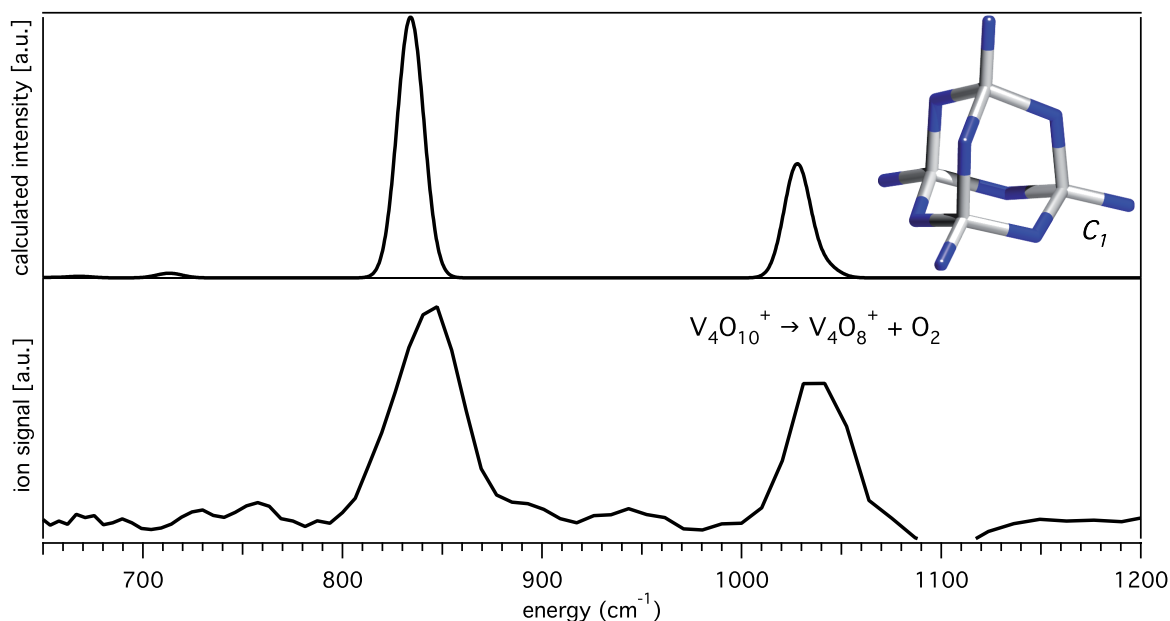

Figure A.1: IR-PD spectrum of $V_4O_{10}^+$ obtained by monitoring the fragment $V_4O_8^+$ production (bottom) and DFT calculations by Vyboishchikov and Sauer [111] for the most stable isomer (top).
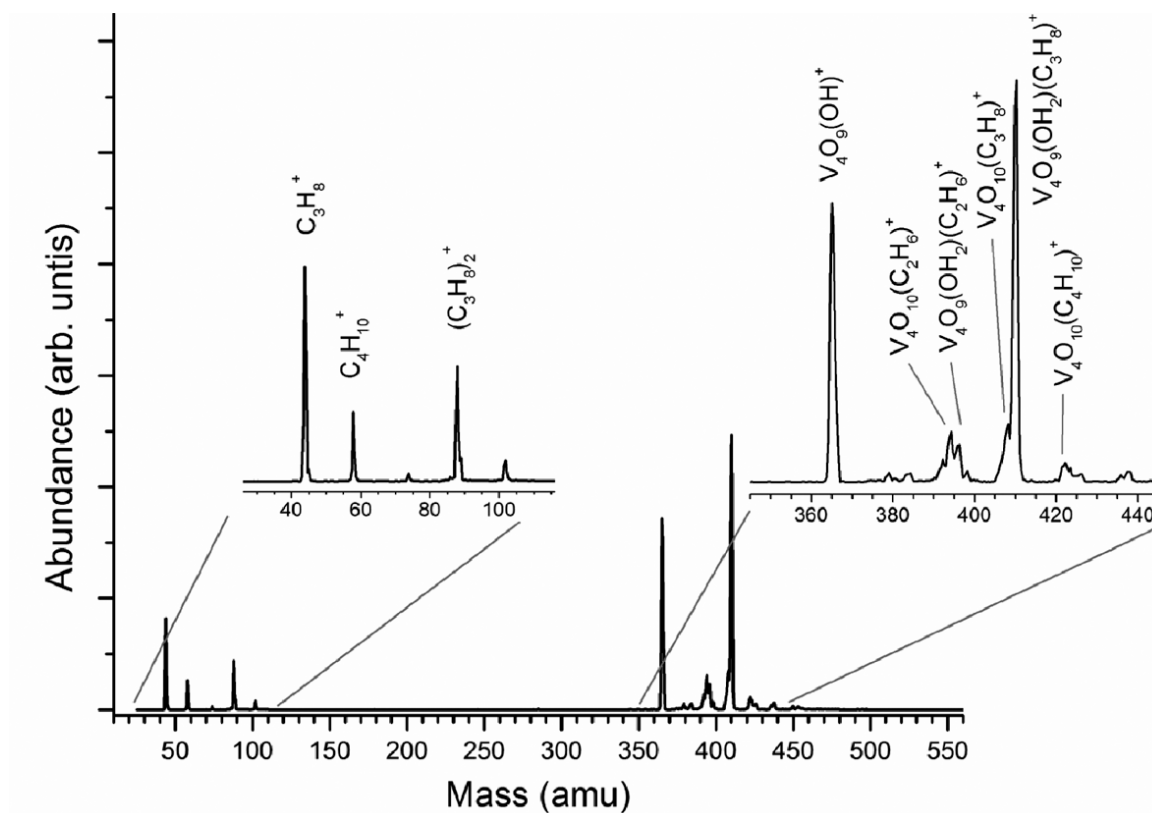
Figure A.2: Mass spectrum of the reaction products after $V_4O_{10}{}^+$ is trapped in the hexadecapole ion trap for 400 ms at a temperature of 110 K with $5\cdot10^{-5}$ mbar.
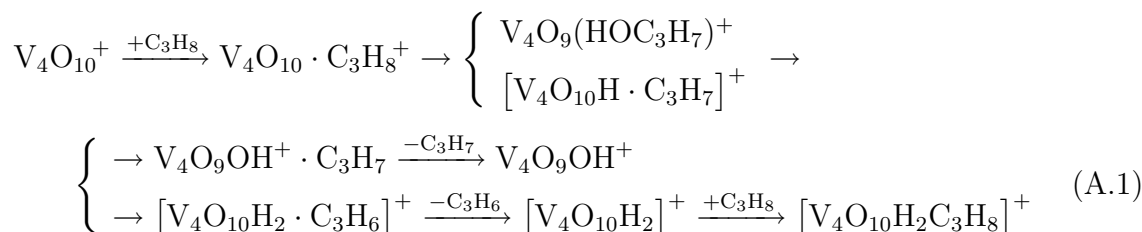
A.2   Experimental Details

The vanadium oxide clusters are produced by pulsed laser vaporization run at 10 Hz. A gas mixture consisting of 1% oxygen in helium is used, yielding oxygen saturated cluster growth conditions. The reaction of mass selected $V_4O_{10}{}^+$ takes place in the hexadecapole ion trap at a temperature of 110 K. Experiments at lower temperature are hindered by propane freezing in the tube that carries the gas to the trap. The trap is filled with 0.006 mbar helium buffer gas containing a fraction of 0.2% of propane. The number of propane molecules is therefore orders of magnitude larger than the number of selected $V_4O_{10}{}^+$ clusters.

A.3   Results

The ion-molecule reaction of $V_4O_{10}{}^+$ with propane results in several reaction products as shown in Figure A.2. Note that the experimental apparatus cannot determine the

identity of neutral species formed during the reaction. The most intense reaction products formally correspond to $[V_4O_9(OH_2)(C_3H_8)]^+$, $[V_4O_{10}H]^+$, and $C_3H_8{}^+$, while the parent ion $V_4O_{10}{}^+$ is not present at all. $[V_4O_{10}H]^+$ might result from oxidative dehydrogenation of the alkane molecule. $C_3H_8{}^+$ can be formed together with the neutral V_4O_{10} cluster upon electron transfer. The largest signal is observed for the formal $[V_4O_9(OH_2)(C_3H_8)]^+$. This complex must be created after multiple reaction steps involving two propane molecules. For example:

$$V_4O_{10}{}^+ \xrightarrow{+C_3H_8} V_4O_{10} \cdot C_3H_8{}^+ \rightarrow \begin{cases} V_4O_9(HOC_3H_7)^+ \\ \left[V_4O_{10}H \cdot C_3H_7 \right]^+ \end{cases} \rightarrow$$

$$\begin{cases} \rightarrow V_4O_9OH^+ \cdot C_3H_7 \xrightarrow{-C_3H_7} V_4O_9OH^+ \\ \rightarrow \left[V_4O_{10}H_2 \cdot C_3H_6 \right]^+ \xrightarrow{-C_3H_6} \left[V_4O_{10}H_2 \right]^+ \xrightarrow{+C_3H_8} \left[V_4O_{10}H_2C_3H_8 \right]^+ \end{cases} \quad \text{(A.1)}$$

Smaller peaks found in the mass spectra, formally corresponding to $[V_4O_{10}(C_3H_8)]^+$, $[V_4O_{10}(C_2H_6)]^+$, and $[V_4O_9(OH_2)(C_2H_6)]^+$, can respectively be assigned to association of propane and C−C bond cleavage reactions. The cleavage reactions most likely occur after a first association and/or dehydrogenation step. There are also small signals related to $C_4H_{10}{}^+$ and $[V_4O_{10}(C_4H_{10})]^+$, which most probably originate from traces of (more reactive) butane rest gas, present in the mixing bottle used for the gas mixture introduced into the ion trap.

It is interesting to compare the present mass spectrum with the reaction products of $V_4O_{10}{}^+$ with propane recorded by Feyel et al. in a hexapole under single collision conditions at room temperature [288]. Opposite to the present findings, the two most pronounced masses found in that study are the bare $V_4O_{10}{}^+$ and the hydrogen transfer product $[V_4O_{10}H_2]^+$. The large difference between the two mass spectra can be attributed to different experimental conditions. First, the present study is performed in an ion trap allowing for long interaction times (about 400 ms), implying multiple cluster-ion collisions, and second, the lower temperature (110 K) enhances the reaction speed (Lindemann mechanism). The $[V_4O_{10}H_2]^+$ species seen by Feyel et al. [288] might be one of the first reaction products that are formed, while the other species of Figure A.2 can be the result of multiple collisions or appear only at longer timescales and lower temperatures.

IR-PD spectra are taken for the most intense $V_4O_{10}{}^+$–molecule complexes present in the trap (with the exception of $[V_4O_{10}H]^+$) after about 400 ms of reaction time and at a temperature of 110 K (see Figure A.2). Absorption of $[V_4O_9(OH_2)(C_3H_8)]^+$ (410 amu) is measured as a wavelength-dependent depletion of the ion signal. Upon depletion of the $[V_4O_9(OH_2)(C_3H_8)]^+$ species, the formation of three fragments is observed: $[V_4O_{10}(C_3H_6)]^+$ (406 amu), $[V_4O_9(C_3H_8)]^+$ (392 amu), and $[V_3O_7(C_3H_8)]^+$ (309 amu). These fragment species are not present in the mass spectra taken without
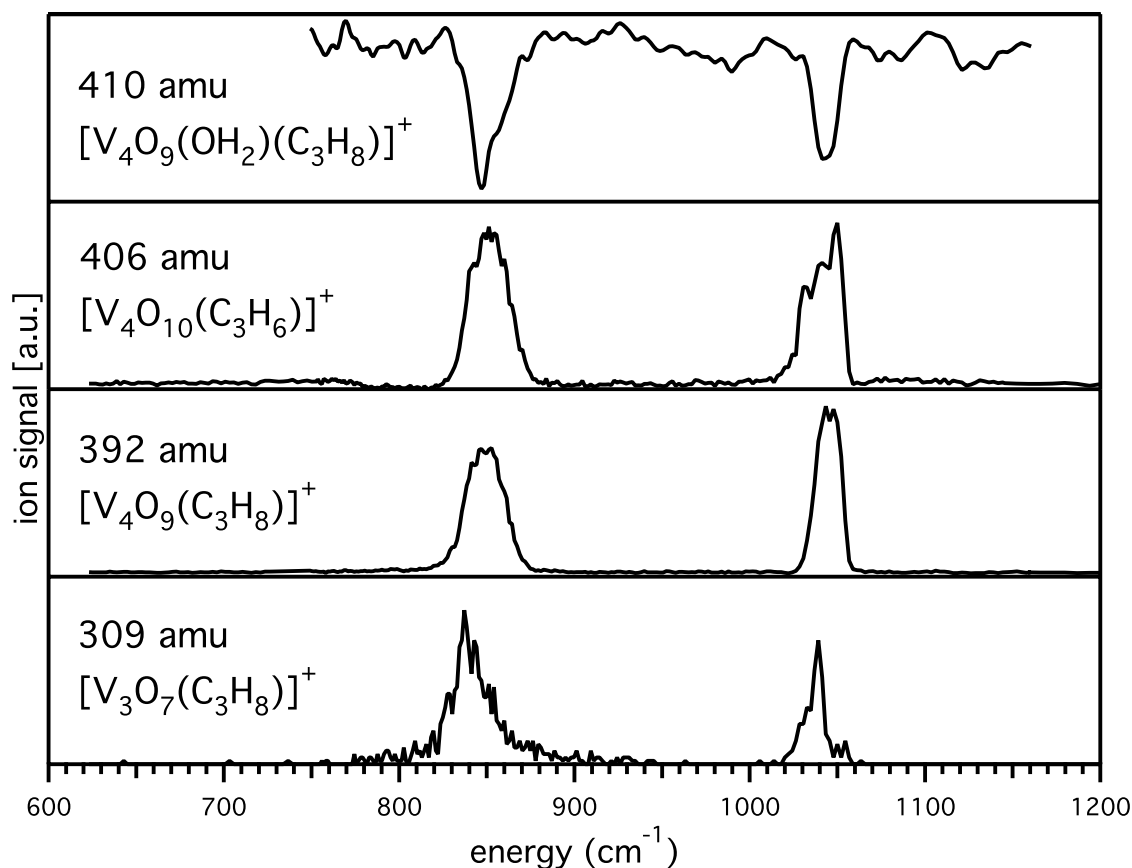
Figure A.3: IR-PD depletion spectrum of $[V_4O_9(OH_2)(C_3H_8)]^+$ (410 amu) and IR-PD formation spectra the three fragments: $[V_4O_{10}(C_3H_6)]^+$ (406 amu), $[V_4O_9(C_3H_8)]^+$ (392 amu), and $[V_3O_7(C_3H_8)]^+$ (309 amu) (from top to bottom).

FELIX and yield, therefore, background free signals. The spectra of these species are shown in Figure A.3. Depletion of the parent signal is monitored for $[V_4O_{10}(C_3H_8)]^+$, $[V_4O_{10}(C_2H_6)]^+$, and $[V_4O_{10}(C_4H_{10})]^+$. The spectra of these species are shown in Figure A.4. For these ions no correspondent fragment formations were observed, presumably because the created fragments are also present without FELIX. A possible fragment can be $[V_4O_{10}H]^+$, for which neither depletion nor formation can be observed.

The IR-PD spectra of the three $V_4O_{10}^+$–alkane complexes, namely $[V_4O_{10}(C_3H_8)]^+$, $[V_4O_{10}(C_2H_6)]^+$, and $[V_4O_{10}(C_4H_{10})]^+$, show remarkable similarities. They are characterized by a multitude of bands, which can roughly be divided into three absorption regions. (*i*) An intense, split peak around 1050 cm^{-1}, (*ii*) the 700–950 cm^{-1} region showing several intense absorption bands, and (*iii*) some weaker bands below 670 cm^{-1}. Combined IR-PD spectroscopy and density functional theory studies on bare vanadium oxide and mixed vanadium-titanium oxide clusters (see Chapters 3, 5,
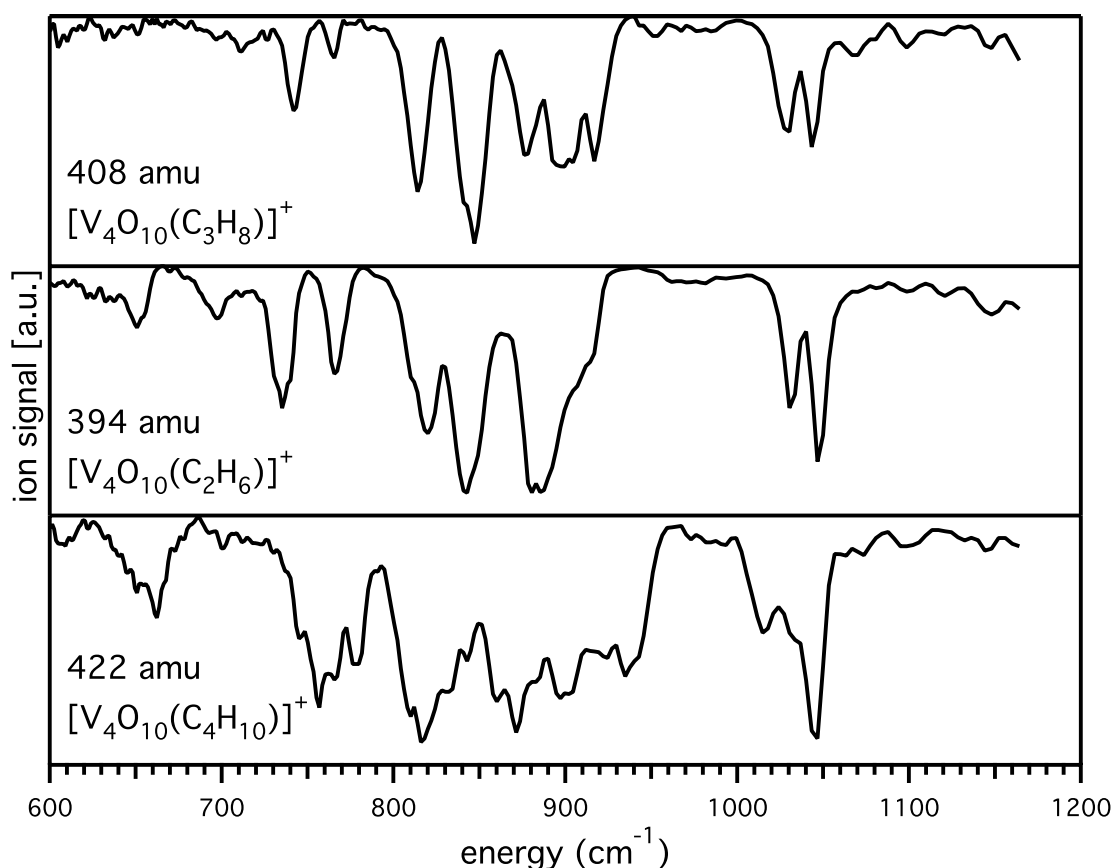
Figure A.4: IR-PD depletion spectra of $[V_4O_{10}(C_3H_8)]^+$ (408 amu), $[V_4O_{10}(C_2H_6)]^+$ (394 amu), and $[V_4O_{10}(C_4H_{10})]^+$ (422 amu) (from top to bottom).

and References [54, 104, 113, 294]) have assigned these absorption regions to the characteristic vibrational modes of (*i*) the vanadyl stretches, (*ii*) the symmetric and asymmetric stretches of the V−O−V bridges, and (*iii*) vibrations involving larger parts of the metal oxide clusters. The IR-PD spectrum obtained for $[V_4O_9(OH_2)(C_3H_8)]^+$ is very different from those found for the other alkane complexes and only shows two sharp bands at 850 and 1050 cm^{-1}. Remarkably, the $[V_4O_9(OH_2)(C_3H_8)]^+$ spectrum strongly resembles the $V_4O_{10}{}^+$ one. The two bands found in the $V_4O_{10}{}^+$ spectrum are less than 10 cm^{-1} red-shifted with respect to the bands of the $[V_4O_9(OH_2)(C_3H_8)]^+$ spectrum [292].

A.4   Discussion

In order to elucidate the reaction mechanism of $V_4O_{10}{}^+$ with propane, IR-PD spectra of the different species present in the ion trap can be compared with DFT calcula-
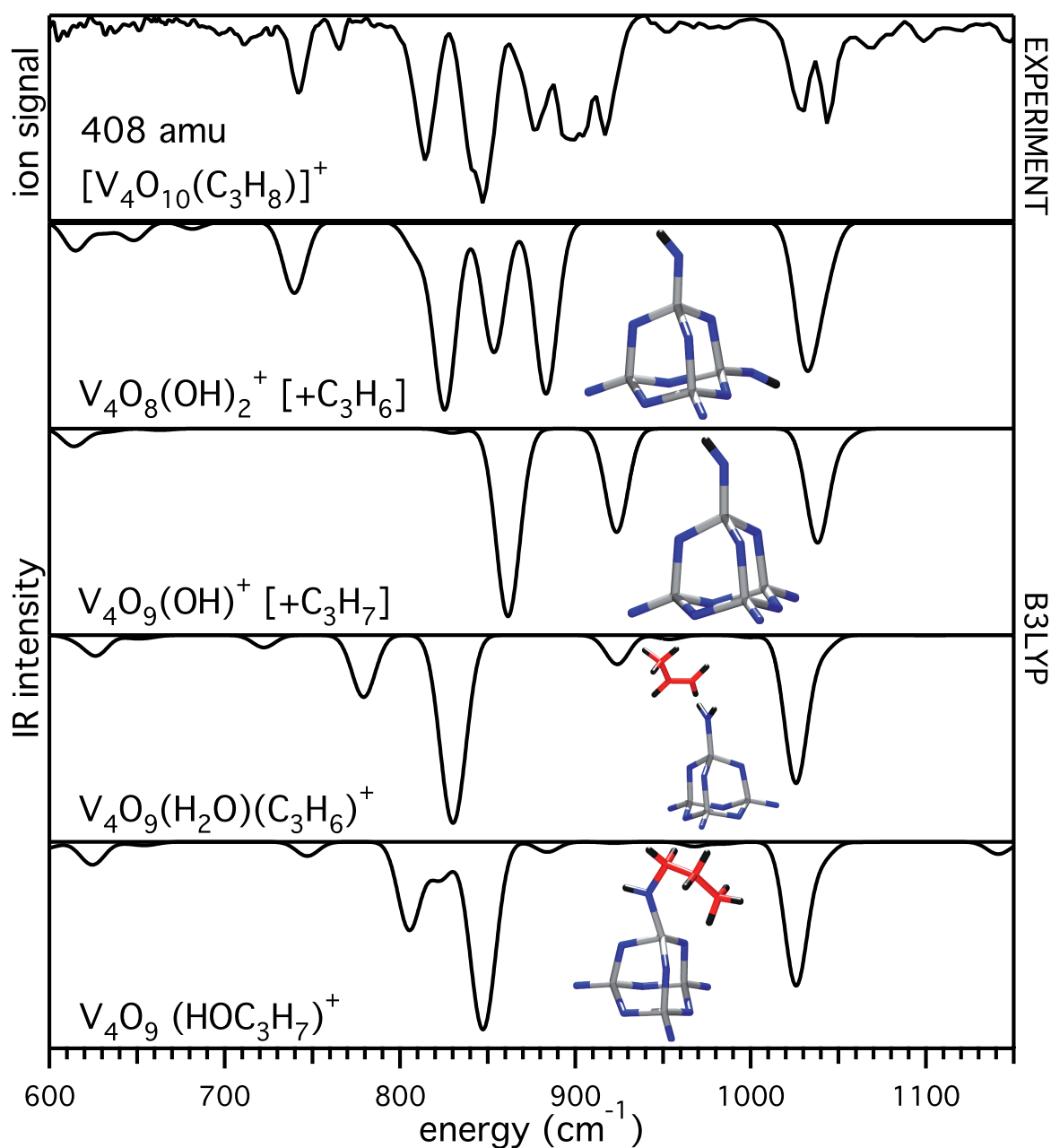
Figure A.5: IR-PD depletion spectrum of $[V_4O_{10}(C_3H_8)]^+$ (408 amu) (top), and DFT calculations for $[V_4O_8(OH_2)_2]^+$, $[V_4O_9(OH_2)]^+$, $[V_4O_9(H_2O)]^+$, and $[V_4O_9(HOC_3H_7)]^+$. The species necessary to reach 408 amu are indicated in brackets. Calculated IR intensities are convoluted with a Gaussian profile (FWHM 18 cm^{-1}) and are plotted as transmission spectra for better comparison with the experimental data.

tions. Sauer and coworkers (Humboldt-Universität zu Berlin, Germany) carried out DFT calculations optimizing the structures of some cluster that can possibly take part in the reaction [197]. In Figure A.5, the depletion spectrum of $[V_4O_{10}(C_3H_8)]^+$ (408 amu) is compared with DFT calculations for $[V_4O_8(OH_2)_2]^+$, $[V_4O_9(OH_2)]^+$, $[V_4O_9(H_2O)(C_3H_6)]^+$, and $[V_4O_9(HOC_3H_7)]^+$. Note that only the last two calculated species have mass 408 amu, therefore, in the other cases, it is assumed that hydrocarbon molecules are present as part of a complex in order to reach mass 408 amu. The typical C$-$C and C$-$H strong absorption bands from the hydrocarbons are at energies higher than the region studied here. However, it is difficult to predict, without calculation for the complete complexes, (i) what effect the perturbation induced by the hydrocarbon molecule should have on the calculated spectrum, and (ii) oscillator strengths of the lower energy modes of the hydrocarbons, which are active in the 600–1200 cm^{-1} region. Therefore, further calculations are needed for a definite structural assignment. Interestingly, reasonable agreement is found between the IR-PD spectrum of $[V_4O_{10}(C_3H_8)]^+$ and calculations for $[V_4O_8(OH_2)_2]^+$. In particular, the two maxima found at 1031 and 1050 cm^{-1} are calculated at 1031 and 1042 cm^{-1}, respectively (they cannot be recognized in the calculated spectrum shown in Figure A.5, which was convoluted with a Gauss profile with FWHM of 18 cm^{-1} for overall better comparison with the experimental data). Discrepancies between calculations and experiment are observed for the broad absorption measured between 850 and 910 cm^{-1}, with maxima at 876, 900, and 917 cm^{-1}, whereas calculations predict a single absorption at 883 cm^{-1}. However, the absorption spectrum of propene—that has to be assumed to be present in the complex in order to reach mass 408 amu—has a strong broad band peaked at 900 cm^{-1} [295] and this could tentatively account for the observed absorption.

The IR-PD depletion spectrum of formal $[V_4O_9(OH_2)(C_3H_8)]^+$ (mass 410 amu) with correspondent formation of the $[V_4O_9(C_3H_8)]^+$ fragment (mass 392 amu) is shown in Figure A.6, together with DFT calculations for the $[V_4O_9(OH_2)(C_3H_8)]^+$ complex. The calculated spectrum is similar to the measured IR-PD spectrum with the exception of the pronounced splitting of the calculated band at 850 cm^{-1}. The harmonic spectrum is calculated at 0 K, meaning that the structure is frozen. The band splitting originates from symmetry-lowering (from C_{3v} to C_s) because of the weakly attached water and propane molecules. At 110 K, the water and the propane moieties can rotate almost freely so that, on average, the system is again symmetric and the splitting of the band at 850 cm^{-1} should be removed. The calculated IR absorption spectrum of $[V_4O_9(OH_2)(C_3H_8)]^+$ is very similar to the one calculated for $[V_4O_9(H_2O)]^+$ (see Figure A.5), and the propane moiety is almost transparent in the 600–1200 cm^{-1} region.
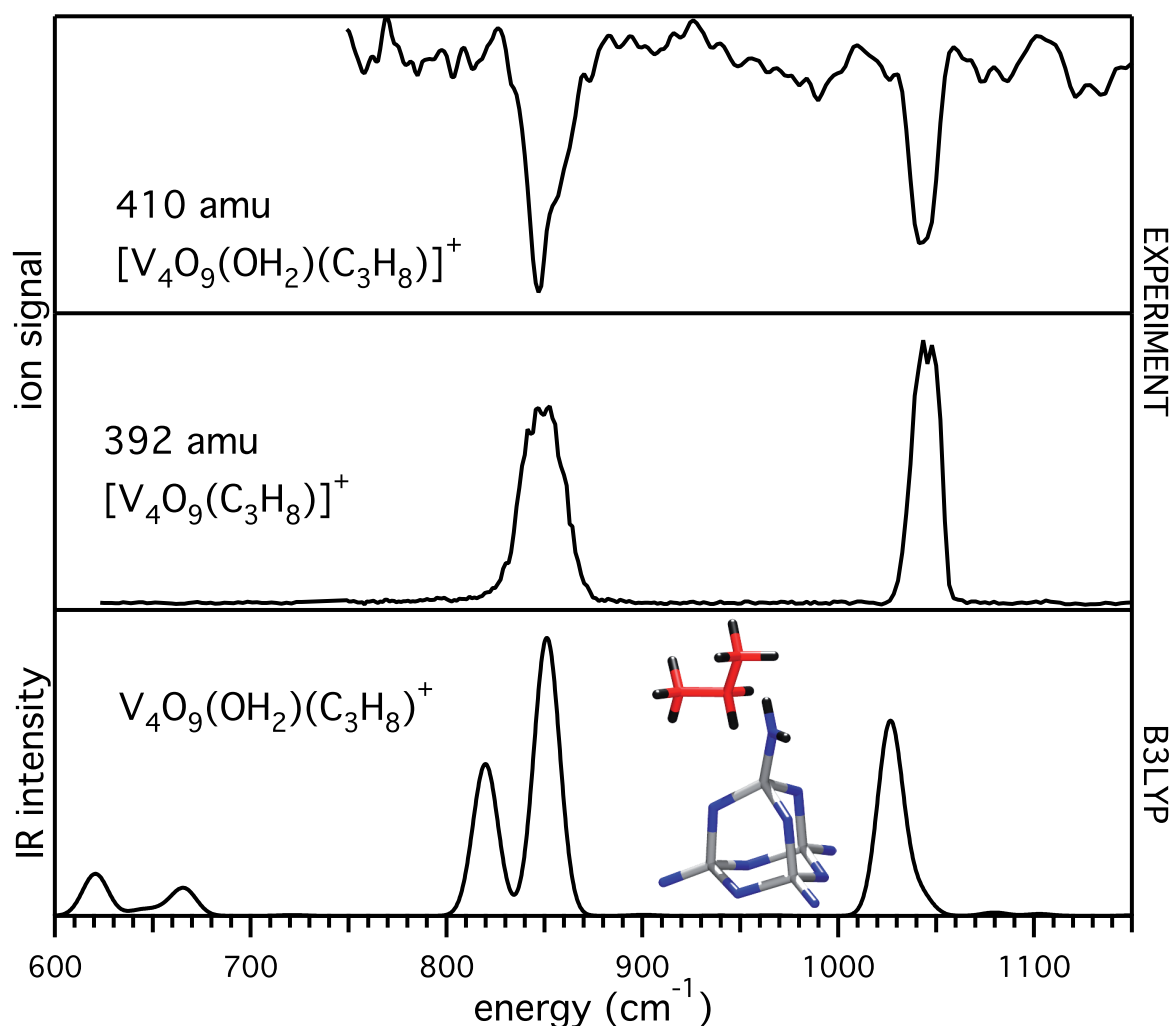
Figure A.6: IR-PD depletion spectrum of $[V_4O_9(OH_2)(C_3H_8)]^+$ (410 amu) (top) and IR-PD formation spectrum of the fragment $[V_4O_9(C_3H_8)]^+$ (392 amu) (center), compared with calculations for $[V_4O_9(OH_2)(C_3H_8)]^+$ (bottom).

A.5 Conclusions

It is difficult to conclude what is the real reaction mechanism on the basis of these preliminary results. Beside further calculations, kinetics studies are necessary, which can be readily performed in the ion trap by tuning temperature, gas concentration, and reaction time [296]. However, the present technique gives a precious piece of information about the structure of reaction participants. In fact, several species are present in equation (A.1) that are indistinguishable by bare mass spectrometry, e.g., the $[V_4O_{10}C_3H_8]^+$ complex (see also Figure A.5).